J. Fluid Mech. (2005), *vol.* 541, *pp.* 1–20.
doi:10.1017/S0022112005006026 Printed in the United Kingdom

Aerodynamic effects in the break-up of liquid jets: on the first wind-induced break-up regime

By J. M. GORDILLO AND M. PÉREZ-SABORID

Área de Mecánica de Fluidos, Departamento de Ingeniería Energética y Mecánica de Fluidos, Universidad de Sevilla, Avda. de los Descubrimientos s/n, 41092, Sevilla, Spain
jgordill@us.es

(Received 21 October 2004 and in revised form 9 May 2005)

We present both numerical and analytical results from a spatial stability analysis of the coupled gas–liquid hydrodynamic equations governing the first wind-induced (FWI) liquid-jet break-up regime. Our study shows that an accurate evaluation of the growth rate of instabilities developing in a liquid jet discharging into a still gaseous atmosphere requires gas viscosity to be included in the stability equations even for low We_g, where $We_g = \rho_g U_l^2 R_0/\sigma$, and ρ_g, U_l, R_0 and σ are the gas density, the liquid injection velocity, the jet radius and the surface tension coefficient, respectively. The numerical results of the complete set of equations, in which the effect of viscosity in the gas perturbations is treated self-consistently for the first time, are in accordance with recently reported experimental growth rates. This permits us to conclude that the simple stability analysis presented here can be used to predict experimental results. Moreover, in order to throw light on the physical role played by the gas viscosity in the liquid-jet break-up process, we have considered the limiting case of very high Reynolds numbers and performed an asymptotic analysis which provides us with a parameter, α, that measures the relative importance of viscous effects in the gas perturbations. The criterion $|\alpha| \ll 1$, with α computed *a priori* using only the much simpler inviscid stability results is a guide to assess the accuracy of a stability analysis in which viscous diffusion is neglected. We have also been able to explain the origin of the *ad hoc* constant 0.175 introduced by Sterling & Sleicher (*J. Fluid Mech.* vol. 68, 1975, p. 477) to correct the discrepancies between Weber's results (*Z. Angew. Math. Mech.* vol. 11, 1931, p. 136) and the experimental ones.

1. Introduction

The stability analysis of liquid jets is relevant for the analysis of several commercial atomization devices and, in particular, for pressure atomizers such as those used in diesel engines, turbojet afterburners, ink-jet printers, etc. In these devices, a high-velocity jet of a given liquid discharges from a circular hole into a stagnant atmosphere, and different breakup regimes present themselves depending on a large number of parameters, such as liquid-jet velocity, nozzle design and gas density. The injector geometry influences the liquid-jet breakup; as pointed out by Reitz & Bracco (1982) and Lin & Reitz (1998), turbulence, liquid velocity profile and cavitation within the nozzle are factors which can decisively affect the breakup of the liquid jet. On the other hand, with regard to the outer atmosphere influence on the jet breakup, Reitz & Bracco (1982) concluded that if the outer gas density is increased and both the

nozzle geometry and the liquid injection velocity are kept constant, the growth rate of perturbations leading to the jet breakup is enhanced.

In the present paper, and in order to isolate the influence of the aerodynamic effects on the jet breakup, we will deal with situations in which the breakup mechanisms associated with cavitation, liquid velocity profile or liquid turbulence are absent. These conditions can be achieved in experimental set-ups such as those reported by Sterling & Sleicher (1975), Kalaaji *et al.* (2003) and González & García (2004), where convergent nozzles with a small length to diameter ratio are used. In these facilities, the liquid-jet exiting the nozzle is laminar and vorticity is confined within a layer, of thickness δ_l, adjacent to the jet interface.

Under these conditions, it is experimentally observed that, for the lower injection velocities, a liquid jet is not formed and a *dripping* regime is obtained owing to surface-tension confinement forces overcoming liquid inertia and gravity (see Clanet & Lasheras 1999; Ambravaneswaran, Phillips & Basaran 2000; Ambravaneswaran *et al.* 2004; Le Dizès 1997; Lin & Lian 1989). If the liquid velocity is progressively increased by keeping the rest of parameters constant, a liquid jet is formed giving rise to a *jetting* regime. For the lower liquid velocities within the jetting regime, the breakup length l_b depends linearly on the injection velocity U_l. This can be explained by Rayleigh's (1878) pioneering investigations. In Rayleigh's analysis, the inertia of the outer atmosphere is not taken into account and, therefore, surface-tension forces are the only ones responsible for instability. However, for a larger injection velocity, we obtain the so-called first wind-induced breakup regime (FWI), for which experiments show that the liquid jet length increases with velocity until it reaches a maximum (Sterling & Sleicher 1975; Lin & Reitz 1998). In these experiments, the shortening in the breakup length that can be solely attributed to aerodynamic effects due to l_b is such that $l_r \ll l_b$, where $l_r \sim U_l\,\delta_l^2/\nu_l$ is the liquid relaxation length and U_l and ν_l are the liquid injection velocity and kinematic viscosity, respectively. The size of the drops in the FWI is still of the order of the jet radius, although smaller than those obtained in the Rayleigh regime.

In spite of all the experimental and theoretical efforts made through the years, Rayleigh's breakup regime is the only one that is perfectly understood. In an attempt to explain the experimental results at larger injection velocities, Weber (1931) extended Rayleigh's work to include the effect of the surrounding gas inertia into the stability analysis. Weber considered a simple Kelvin–Helmholtz model, uniform liquid and gas velocity profiles, and retained viscosity only in the liquid linear stability equations. He found that the inclusion of aerodynamic effects into the analysis predicts, as observed experimentally, a maximum in the curve of breakup length *vs.* injection velocity. However, the maximum predicted by this theory occurs for lower velocities than those measured experimentally, which led Sterling & Sleicher (1975) to extend the analysis by including the effect of the gas viscosity. For this purpose, they introduced an *ad hoc* parameter whose effect is to reduce the perturbed gas pressure at the jet interface. The value of this parameter (0.175) was adjusted so that the predicted breakup lengths agreed with the experimental ones. It has been shown that the growth rates, measured under controlled experimental conditions Kalaaji *et al.* 2003; González & García 2004, are reproduced well assuming this *ad hoc* attenuation constant. The good agreement with the experiments suggests that the Sterling & Sleicher (1975) approximation to account for gas viscosity, is conceptually valid. However, in spite of the importance of the FWI breakup regime for numerous applications, there is still no study in the literature that includes, self-consistently, the effect of gas viscosity in the equations governing the liquid-jet breakup.

As pointed out above, the condition $l_b \gg l_r$, which is implicitly assumed in this study, is experimentally achieved in experimental set-ups such as those reported by Sterling & Sleicher (1975), Kalaaji *et al.* (2003) and González & García (2004), but only within a certain velocity range. Indeed, if the liquid velocity is sufficiently high, the liquid jet starts breaking up only a few diameters downstream of the nozzle, giving rise to the so-called second wind-induced break-up regime, and a further increase in the liquid velocity leads to the atomization regime, where the breakup of the jet starts at the injector outlet. In both the second wind-induced and the atomization regimes, the drops obtained are much smaller than the orifice diameter and $l_r \lesssim O(l_b)$. Consequently, the liquid velocity profile (see Hoyt & Taylor 1977; Yoon & Heister 2004), the possible cavitation of the liquid within the nozzle and the aerodynamic interaction with the surrounding atmosphere, play a role in the breakup process under these experimental conditions. See Reitz & Bracco (1982) and Lin & Reitz (1998) and references therein for a more detailed quantitative description of these regimes since they are out of the scope of this study.

In the framework of co-flowing liquid–gas jets it has been shown that, in the limit of high Reynolds numbers, the primary instability mechanism leading to atomization is controlled, for large values of the momentum ratio, $M = \rho_g U_g^2/\rho_l U_l^2$, by the gas shear-layer thickness (Villermaux 1998; Lasheras & Hopfinger 2000; Marmottant & Villermaux 2004) and, in the case of $M \lesssim 1$, by the liquid shear-layer thickness (Hoyt & Taylor 1977; Gordillo, Pérez-Saborid & Gañán Calvo 2001). In the above-cited studies, liquid and gas viscosities only enters into the analysis through the liquid and gas basic velocity profiles. However, in the more theoretical approach by Lin & Chen (1998) and Yecko, Zaleski & Fullana (2002), viscosity was also considered in the equations governing the perturbations; moreover, the importance of interfacial shear in the development of instabilities leading to atomization was also stressed. In the context of the atomization of planar liquid sheets Lozano *et al.* (2001) also retain gas viscosity both in the basic state and in the stability equations.

The purpose of the present paper is to solve, by including gas viscosity in a self-consistent manner, the stability equations modelling the breakup of a liquid jet injected into a still air atmosphere in the cases in which liquid velocity profile relaxation effects can be neglected. It will be shown that the results of the present analysis and the experimentally measured growth rates provided by Kalaaji *et al.* (2003) are in excellent agreement and thus, a simple stability analysis such as the one presented here, can be used to predict experimental results. Furthermore, the role played by gas viscosity has been elucidated by performing an asymptotic analysis that recovers the numerical results for sufficiently high Reynolds numbers. The asymptotics show that the role played by gas viscosity can be split in two separate effects: On the one hand, at zeroth order, viscosity generates a gas boundary layer surrounding the liquid jet that diminishes the aerodynamic interaction between the liquid jet and the surrounding atmosphere with respect to the Kelvin–Helmholtz model (Gordillo *et al.* 2001). On the other hand, for sufficiently high Reynolds numbers, viscous effects in the perturbed quantities are confined to Stokes layers developing at the jet surface as a consequence of the continuity of velocities across the interface.

The paper is structured as follows: in § 2, we formulate the equations governing the basic flow and the perturbations and compare the numerical with the experimental results. Section 3 is devoted to the asymptotic stability analysis and a comparison between numerical and asymptotic results is provided. Finally, conclusions are presented in § 4.

2. Formulation of the problem and numerical results

A liquid jet discharging into a still gaseous atmosphere generates a boundary-layer type of flow in the surrounding medium which is induced by gas viscosity. It will be shown that the growth of the perturbations leading to the jet breakup strongly depends on the basic gas velocity field and, consequently, a correct computation of the downstream evolution of the gas boundary layer is essential for the subsequent analysis.

The basic flow has been computed assuming that the liquid velocity profile, U_l, is uniform and the radius of the jet, R_0, constant. This approach is consistent since relaxation effects in the liquid velocity profile can be neglected under the experimental conditions leading to the FWI breakup regime (Sterling & Sleicher 1975; Kalaaji *et al.* 2003; González & García 2004); moreover, the influence of the gas viscous shear in the liquid velocity profile will be small since

$$\mu_g/\mu_l \ll 1, \tag{2.1}$$

where the subscripts l and g in (2.1) indicate liquid and gas, respectively. In addition, accelerations due to gravity are neglected since, either gravity is transversal to the flow direction (Sterling & Sleicher 1975) or $Fr = U_l^2/g\,l_b \gg 1$ in the experiments considered here. Indeed, even in the most unfavourable case, consistent with the experimental conditions reported in Sterling & Sleicher (1975) and Kalaaji *et al.* (2003) that $l_b \sim 10^2 R_0$, $R_0 \sim 10^{-3}$ m and $U_l \sim 10\,\mathrm{m\,s^{-1}}$, the Froude number is such that $Fr \sim 10^2 \gg 1$.

In the high-Reynolds-number limit, $Re_g = U_l\,R_0/\nu_g = Re\,(\nu_l/\nu_g) \gg 1$, the dimensionless continuity and momentum equations governing the basic gas flow in cylindrical coordinates read

$$\frac{\partial U_g}{\partial z_g} + \frac{1}{\xi}\frac{\partial(\xi V_g)}{\partial \xi} = 0, \tag{2.2}$$

$$U_g\frac{\partial U_g}{\partial z_g} + V_g\frac{\partial U_g}{\partial \xi} = \frac{1}{\xi}\frac{\partial}{\partial \xi}\left(\xi\frac{\partial U_g}{\partial \xi}\right), \tag{2.3}$$

where $\xi = r/R_0$ and $z_g = z\nu_g/U_l\,R_0^2$. Moreover, the characteristic scales used to define the dimensionless axial (U_g) and radial (V_g) gas velocity components are U_l and ν_g/R_0, respectively. The solution to the system (2.2)–(2.3), which must be solved subjected to the boundary conditions,

$$z = 0, \quad U_g = U_g(\xi, 0), \tag{2.4}$$

$$\xi = 1, \quad U_g = 1, \quad V_g = 0, \quad \xi \to \infty \quad U_g \to 0, \tag{2.5}$$

has been obtained through the numerical procedure described in Gordillo *et al.* (2001) and has been checked against that of the flow along a cylinder provided in Tutty, Price & Parsons (2002). Note that the condition for the axial velocities in (2.4) is taken to be the self-similar Blasius-type solution describing the boundary layer forming at a flat plate emerging normally to a wall (Rodríguez-Rodríguez, Sánchez & Martínez-Bazán 2004). It has to be pointed out that this initial condition is also valid in the case where the jet emerges directly from a nozzle which is not bounded by a rigid wall.

Figures 1(a) and 1(b) show, respectively, the growth of the gas boundary-layer thickness and the decrease of the shear stress, $\tau_f = \partial U_g/\partial\xi(\xi = 0)$, along the liquid-jet interface. Note that the solution obtained is free of parameters and, consequently, (2.2)–(2.5) need to be solved only once. Moreover, although this solution does not satisfy the continuity of the shear stress at the interface, the calculated growth rates are in close agreement with the experimental ones, as will be shown below.

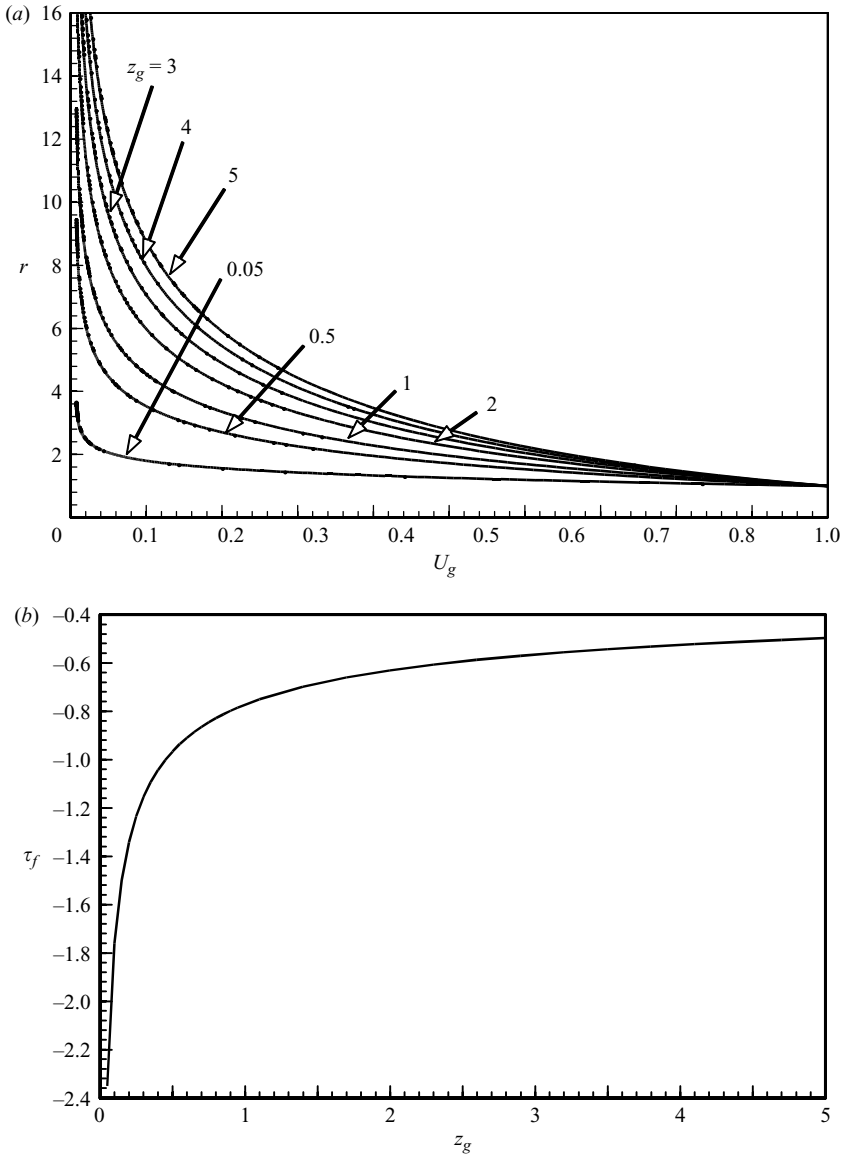

FIGURE 1. (*a*) Gas velocity profiles at different axial positions. Note the downstream growth of the boundary layer. (*b*) Shear stress along the liquid jet interface.

The evolution of the perturbations along the liquid jet is solved by linearizing the Navier–Stokes equations around the already obtained gas and liquid basic states. Since the basic flow is essentially non-parallel, any of the dimensionless perturbed axial, radial and azimuthal velocity components ($u_{l,g}$, $v_{l,g}$, $w_{l,g}$) and pressure fields $p_{l,g}$ can be expressed, in the usual WKB decomposition (Bertolotti, Herbert & Spalart 1992; Fernández-Feria 1999) as $q(\xi, z_l, \tau, \theta) = \bar{q}(\xi, z_l)\chi(z_l, \tau, \theta)$, being

$$\chi(z_l, \tau, \theta) = \exp\left[\mathrm{i}\left(Re\int_0^{z_l} k(\zeta)\,\mathrm{d}\zeta - \Omega\tau + m\theta\right)\right], \tag{2.6}$$

and θ the azimuthal angle. The dimensionless axial coordinate is defined as $z_l = z/ReR_0$, where $Re = U_l R_0/\nu_l$ is the Reynolds number. The characteristic length and velocity scales used to define the dimensionless velocity, time (τ), frequency (Ω) and wavenumber (k) are R_0 and U_l, respectively; perturbed gas and liquid pressures are made non-dimensional using $\rho_l U_l^2$ and $\rho_g U_l^2$ as characteristic scales. Introducing perturbations of the form (2.6) into the linearized Navier–Stokes equations and retaining terms up to order $1/Re$, the equations governing the variables $(u_{l,g}, v_{l,g}, w_{l,g}, p_{l,g})$ read, with $b \equiv \mathrm{i}k$,

$$\frac{1}{Re}\frac{\partial u_{l,g}}{\partial z_l} = -b u_{l,g} - \left(\frac{\partial v_{l,g}}{\partial \xi} + \frac{v_{l,g}}{\xi} + \frac{\mathrm{i}m\, w_{l,g}}{\xi}\right), \tag{2.7}$$

$$\begin{aligned}\frac{1}{Re}U_{l,g}\frac{\partial v_{l,g}}{\partial z_l} = {} & \mathrm{i}\Omega\, v_{l,g} - \frac{\partial p_{l,g}}{\partial \xi} \\ & + \frac{1}{Re}\left[-(\nu_{l,g}/\nu_l)\frac{\partial V_{l,g}}{\partial \xi} - b\,Re\,U_{l,g} - (\nu_{l,g}/\nu_l)\left(\frac{1+m^2}{\xi^2} - b^2\right)\right] v_{l,g} \\ & + \frac{1}{Re}\left(-(\nu_{l,g}/\nu_l)\,V_{l,g} + \frac{(\nu_{l,g}/\nu_l)}{\xi}\right)\frac{\partial v_{l,g}}{\partial \xi} \\ & + \frac{(\nu_{l,g}/\nu_l)}{Re}\frac{\partial^2 v_{l,g}}{\partial \xi^2} - \frac{2\mathrm{i}m\, w_{l,g}(\nu_{l,g}/\nu_l)}{Re\,\xi^2},\end{aligned} \tag{2.8}$$

$$\begin{aligned}\frac{1}{Re}U_{l,g}\frac{\partial w_{l,g}}{\partial z_l} = {} & \mathrm{i}\Omega\, w_{l,g} - \frac{\mathrm{i}m\, p_{l,g}}{\xi} + \frac{1}{Re}\left[-(\nu_{l,g}/\nu_l)\frac{V_{l,g}}{\xi} - b\,Re\,U_{l,g}\right. \\ & \left. - (\nu_{l,g}/\nu_l)\left(\frac{1+m^2}{\xi^2} - b^2\right)\right] w_{l,g} + \frac{1}{Re}\left(-(\nu_{l,g}/\nu_l)\,V_{l,g} + \frac{(\nu_{l,g}/\nu_l)}{\xi}\right)\frac{\partial w_{l,g}}{\partial \xi} \\ & + \frac{(\nu_{l,g}/\nu_l)}{Re}\frac{\partial^2 w_{l,g}}{\partial \xi^2} + \frac{2\mathrm{i}m\,(\nu_{l,g}/\nu_l)\,v_{l,g}}{Re\xi^2},\end{aligned} \tag{2.9}$$

$$\begin{aligned}\frac{1}{Re}\frac{\partial p_{l,g}}{\partial z_l} = {} & \mathrm{i}\Omega\, u_{l,g} - b\, p_{l,g} + \frac{1}{Re}\left[-\frac{\partial U_{l,g}}{\partial z_l} - (\nu_{l,g}/\nu_l)\left(\frac{m^2}{\xi^2} - b^2\right)\right] u_{l,g} \\ & + \frac{1}{Re}\left(-(\nu_{l,g}/\nu_l)\,V_{l,g} + \frac{(\nu_{l,g}/\nu_l)}{\xi}\right)\frac{\partial u_{l,g}}{\partial \xi} + \frac{(\nu_{l,g}/\nu_l)}{Re}\frac{\partial^2 u_{l,g}}{\partial \xi^2} \\ & + \left(-\frac{\partial U_{l,g}}{\partial \xi} + \frac{U_{l,g}}{\xi}\right) v_{l,g} + U_{l,g}\frac{\partial v_{l,g}}{\partial \xi} + \frac{\mathrm{i}m\, U_{l,g}}{\xi}\, w_{l,g}.\end{aligned} \tag{2.10}$$

Note that (2.7) is the linearized continuity equation and (2.8)–(2.10) stand for the radial, azimuthal and axial components of the linearized momentum equation, respectively. The system (2.7)–(2.10) must be solved subjected to the following boundary conditions at $\xi = 0$,

$$\text{if} \quad m = 0, \quad \frac{\partial u_l}{\partial \xi} = 0, \quad v_l = w_l = 0, \quad \frac{\partial p_l}{\partial \xi} = 0, \tag{2.11}$$

$$\text{if} \quad m = 1, \quad u_l = p_l = 0, \quad \frac{\partial v_l}{\partial \xi} = 0, \quad \mathrm{i}\, v_l - w_l = 0, \tag{2.12}$$

$$\text{if} \quad m > 1, \quad u_l = v_l = w_l = p_l = 0. \tag{2.13}$$

In addition, the linearized kinematic conditions to be satisfied by the perturbations at the gas–liquid interface, which is located at $\xi = 1 + f(z_l)\,\chi(z_l, \tau, \theta)$, are the continuity of the velocity across the interface and the free-surface condition, respectively,

given by

$$\xi = 1: \quad u_g = u_l - \frac{\partial U_g}{\partial \xi} f, \quad v_g = v_l, \quad w_g = w_l, \tag{2.14}$$

$$\frac{1}{Re}\frac{\partial f}{\partial z_l} = (\mathrm{i}\,\Omega - b)\ f + v. \tag{2.15}$$

The force balance at the interface leads to the next set of dynamic conditions to be satisfied at $\xi = 1$,

$$-\frac{\mu_g}{\mu_l}\frac{\partial^2 U_g}{\partial \xi^2} f + \left(\frac{\partial u_l}{\partial \xi} - \frac{\mu_g}{\mu_l}\frac{\partial u_g}{\partial \xi}\right) + b\left(v_l - \frac{\mu_g}{\mu_l} v_g\right) = 0, \tag{2.16}$$

$$\mathrm{i}m\left(v_l - \frac{\mu_g}{\mu_l} v_g\right) + \left(\frac{\partial w_l}{\partial \xi} - \frac{\mu_g}{\mu_l}\frac{\partial w_g}{\partial \xi}\right) - \left(w_l - \frac{\mu_g}{\mu_l} w_g\right) = 0, \tag{2.17}$$

$$p_l - \frac{\rho_g}{\rho_l} p_g - \frac{2}{Re}\left(\frac{\partial v_l}{\partial \xi} - \frac{\mu_g}{\mu_l}\frac{\partial v_g}{\partial \xi}\right) - \frac{2\mu_g}{\mu_l Re}\frac{\partial U_g}{\partial \xi} b\, f + f\, We^{-1}(1 - m^2 - b^2 + 2\,\mathrm{i}\Omega b) + 2bWe^{-1} v = 0, \tag{2.18}$$

where (2.16)–(2.17) stand for the continuity of the tangential shear stress across the interface and (2.18) is the normal stress jump condition. In (2.18), the Weber number is defined as $We = \rho_l U_l^2 R_0/\sigma$, with σ the surface tension coefficient. Furthermore, in order to compare with experiments, it proves convenient to define at this point the Ohnesorge number, $Oh = \sqrt{We}/Re$.

The resulting system (2.7)–(2.18) gives rise to a set of parabolized stability equations (PSE), which could be solved using the method proposed by Bertolotti *et al.* (1992). However, these authors also show that the solution provided by the PSE method differs, for sufficiently high Reynolds numbers, only slightly from that obtained by the approach which consists in setting to zero the left-hand side terms of (2.7)–(2.10) and (2.15), $(1/Re\,\partial/\partial z_l \equiv 0)$ and solving the local eigenvalue problem at different axial locations. In this paper we have chosen the latter approach since it is easier to implement and not very expensive in terms of computing time. Thus, given Ω, the velocity profiles at an axial position z_g, and the set of parameters We, Re, ρ_g/ρ_l, μ_g/μ_l, equations (2.7)–(2.18) have been discretized using a Chebychev spectral collocation method (Lin & Chen 1998; Yecko *et al.* 2002), for which liquid and gas domains have been mapped into the Chebychev space $\eta \in [-1, 1]$ through the transformations

$$\left.\begin{aligned} &\xi = \tfrac{1}{2}(\eta + 1) \quad \text{for} \quad 0 \leqslant \xi \leqslant 1, \\ &\xi = \frac{2L + 1 - \eta}{L(1 + \eta)} \quad \text{with} \quad L = -\frac{1 + \sqrt{2}/2}{2 - (1 + 10\sqrt{z_g})(1 - \sqrt{2}/2)} \quad \text{for} \quad \xi > 1. \end{aligned}\right\} \tag{2.19}$$

The purpose of the chosen transformation for the gas domain is to cluster as many discrete points as possible within the gas boundary layer, whose thickness is estimated as $\sim O(10\sqrt{z_g})$. Moreover, the spatial gas and liquid domains are discretized using 60 and 25 points, respectively, since usual convergence tests showed that an increase in the number of points did not result in a significant improvement of the results.

The nonlinear eigenvalue problem in k has been solved through the routine DGVCC of the IMSL library once it is transformed into a linear one using the matrix companion method (Bridges & Morris 1984). In order to validate the numerical implementation, we have reproduced both the critical Reynolds numbers for the boundary layer along a cylinder provided in table 1 of Tutty *et al.* (2002) and the eigenvalue

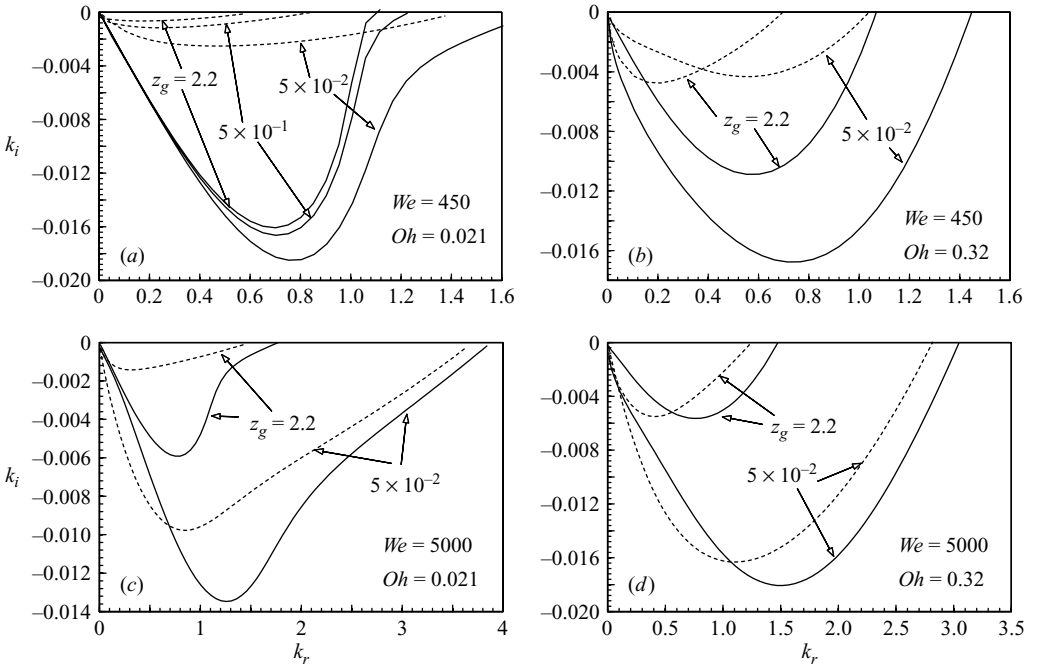

FIGURE 2. $\Omega_i = 0$ isocontours in the (k_r, k_i) complex plane for both axisymmetric ($m = 0$, continuous line) and asymmetric ($m = 1$, dotted line) at different axial positions and for several Weber and Ohnesorge numbers.

corresponding to the atomization conditions considered by Lin & Chen (1998) in their table 1, once we noticed that the calculated results in that table corresponded to a value of the Weber number of 10^6.

Since our final purpose is to compare the computed growth rates with those measured under well-controlled experimental conditions, the values of the control parameters are calculated assuming the same physical properties of the liquids used by Kalaaji *et al.* (2003), with $\rho_a = 1.2\,\mathrm{kg\,m^{-3}}$, $\nu_a = 1.5 \times 10^{-5}\,\mathrm{m^2\,s^{-1}}$. Moreover, the range of values of the parameters defining the operating conditions (Re, We and z_g) are calculated consistently with the experimental situations under which the growth rates provided in figure 8 of Kalaaji *et al.* (2003) are measured.

Figure 2 represents several $k(\Omega)$ isocontours ($\Omega_i = 0$) in the complex wavenumber plane for both axisymmetric ($m = 0$) and asymmetric ($m = 1$) unstable modes at several axial locations and different values of both Weber and Ohnesorge numbers. The instability is convective owing to the range of Weber numbers considered being well within the jetting parametric region (see Ambravaneswaran *et al.* 2004), and the same conclusion can be drawn from the fact that the isocontours in figure 2 do not exhibit a cusp singularity (Olendraru *et al.* 1999). Consequently, from the point of view of linear stability theory, the downstream propagation and growth of disturbances excited at a frequency Ω from the exit nozzle is equivalent to solving the so-called signalling problem by Huerre & Monkewitz (1990) downstream of the excitation source. In order to show that the $k(\Omega)$ branches shown in figure 2 correspond to downstream growing modes we have, at least, two different alternatives. The classic procedure, described by Huerre & Monkewitz (1990), consists in solving $k(\omega)$ for values of $\omega = \omega_r + \mathrm{i}\,\omega_\mathrm{i} = \Omega + \mathrm{i}\,\omega_i$ such that $\mathrm{Im}(\omega) \geqslant 0$. Using causality arguments, Huerre & Monkewitz (1990) showed that only those roots $k^+(\Omega)$ such that the sign of

$\mathrm{Im}[k^+(\omega)]$ change from positive to negative if $\mathrm{Im}(\omega)$ is lowered from a positive value to zero, represent downstream spatially growing waves of the type $\mathrm{e}^{\mathrm{i}(k^+(\Omega)z-\Omega t)}$. Another alternative procedure to identify whether the already obtained eigenvalue $k(\Omega)$ is relevant to describe the response to a periodic forcing of frequency Ω downstream or upstream of the excitation source, consists in determining the sign of the group velocity $\mathrm{d}\omega/\mathrm{d}k$ at the local extremum of the already obtained curve $k(\Omega)$. Note that the extremum is located at a value of Ω_m such that $\mathrm{d}k_i/\mathrm{d}\Omega(\Omega_m)=0$ and, consequently, the group velocity is real and can be calculated as $[\mathrm{d}k_r(\Omega)/\mathrm{d}\Omega(\Omega_m)]^{-1}$. Indeed, using the method of steepest descent, Gordillo & Pérez-Saborid (2002) showed that the spatial eigenvalues $k^+(\Omega)$, relevant for the large-time response downstream of the source (rays $x/t\to 0^+$), are those included in a curve $k(\Omega)$ such that $\mathrm{d}k_r(\Omega)/\mathrm{d}\Omega(\Omega_m)>0$. We have chosen this latter alternative because all the information needed to decide whether the spatial eigenvalues $k(\Omega)$ are relevant for the downstream or upstream response to the periodic forcing at a real frequency Ω, is contained in the already calculated curve $k(\Omega)$. Thus, no more eigenvalues $k(\omega)$, for complex ω need be calculated.

Consequently, owing to $\mathrm{d}k_r(\Omega)/\mathrm{d}\Omega(\Omega_m)\simeq 1>0$ at the maximum of each isocontour represented in figure 2, the spatial branches depicted in this figure correspond to downstream convectively unstable modes. From figure 2 also observe that, given a mode, *We* and *Oh*, both the maximum spatial amplification and the range of unstable wavenumber increases for decreasing z_g, this being a consequence of the fact that, the thicker the gas boundary layer is (the larger z_g is), the smaller is the aerodynamic effect. Figure 2 also shows that the axisymmetric mode growth rate is larger than that of their asymmetric counterparts for wavelengths of the order of that of the radius. Contrarily, asymmetric modes grow faster than the axisymmetric ones for long wavelengths. Moreover, except for the larger values of both the Weber and Ohnesorge numbers ($We=5000$, $Oh=0.32$), the maximum of the spatial amplification varying Ω and keeping the rest of parameters constant, correspond to axisymmetric modes. This result indicates that asymmetric disturbances may grow faster than axisymmetric ones for sufficiently large values of both the Weber number (what is in qualitative agreement with Yang 1992) and of the Ohnesorge number.

In view of the above conclusions it is to be expected that for moderate Weber numbers and in the case of naturally excited jets, the jet breaks up owing to the combined growth of both axisymmetric and long-wavelength helicoidal ($m=1$) perturbations, consistent with Hoyt & Taylor (1977) observations. However, in spite of the considerations concerning helicoidal modes, only $m=0$ cases are to be studied in what follows, since we will deal with experiments in which the jet is excited axisymmetrically.

The spatial amplification factor $-k_{\mathrm{i}}$, which is calculated for the experimental frequencies considered by Kalaaji *et al.* (2003), is a decreasing function of the axial coordinate z_g as depicted in figure 3(*a*). As pointed out above, this is mainly due to the fact that the boundary-layer growth smoothes the velocity gradients in the gas and, consequently, the aerodynamic effect of the surrounding atmosphere diminishes. However, we postpone a full discussion about the role of gas viscosity on the development of the instability to § 3, where it will be shown that gas viscosity must be retained in the perturbed equations in order to reproduce the experimental results. Also relevant in figure 3(*a*) is the fact that the spatial amplification growth rates reach, sufficiently far downstream, their corresponding values in vacuum, which are represented in this figure as horizontal lines. This is consistent with the large boundary-layer thickness (see figure 1*a*) which yields negligible aerodynamic effects (Gordillo *et al.* 2001). The eigenfunctions corresponding to an intermediate axial position $z_g=4.95\times 10^{-2}$ under the same conditions as figure 3(*a*) can be depicted in figure 3(*b*).

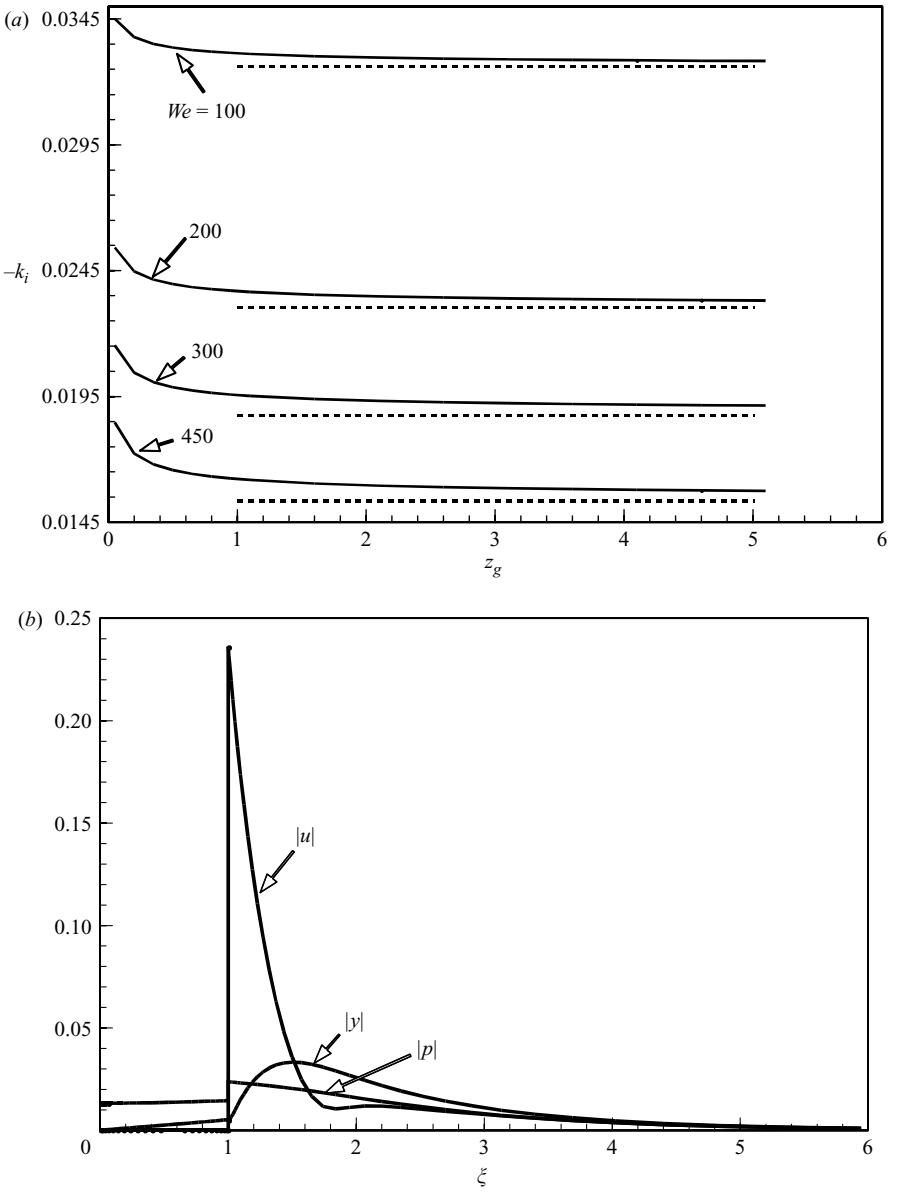

FIGURE 3. (*a*) Downstream evolution of the spatial amplification growth rate, $-k_\mathrm{i}$ for different values of the Weber number. Dashed lines indicate the growth rates in vacuum. $Oh = 0.021$, $\Omega = 0.74$ and physical properties corresponding to those of water and air. (*b*) Eigenfunctions at $z_g = 4.95 \times 10^{-2}$ for $We = 50$, $Oh = 0.021$, $\Omega = 0.74$ and physical properties corresponding to those of water and air.

Once the axial evolution of the spatial amplification has been obtained, and given a dimensionless breakup length z_g^b, the averaged perturbation growth rate $\bar{k}_\mathrm{i}$, can be computed, making use of (2.6) as

$$\bar{k}_\mathrm{i} = \frac{1}{z_g^b} \int_0^{z_g^b} k_i(z_g)\, \mathrm{d}z_g. \tag{2.20}$$

This quantity can be easily measured experimentally once the amplitude of the jet radius (ϵR_0) at $z_g = 0$ and the break-up length $l_b = Re_g R_0 z_g^b$, with $Re_g = U_l R_0/\nu_g$, are known. In effect, since the nonlinearities are confined to only a narrow region close to the breakup point,

$$\bar{k}_{\mathrm{i}} = \ln(\epsilon)\frac{R_0}{l_b}. \tag{2.21}$$

However, the different experimental studies in the literature (see Kalaaji *et al.* 2003; Sterling & Sleicher 1975; González & García 2004) usually provide the value of the dimensionless temporal growth rate $\Omega_i = \omega_i(\rho\, R_0^3/\sigma)^{1/2}$, ω_i being its dimensional counterpart, instead of that of (2.21). Consequently, we have transformed our results making use of the Gaster approximation (Gaster 1962),

$$\Omega_i = \bar{k}_i We^{1/2}, \tag{2.22}$$

where the validity of (2.22) is ensured since, in the experimental conditions under consideration, the Weber number is sufficiently high for the group velocity to be approximated to U_l (Keller, Rubinow & Tu 1973). Note that the averaged perturbation growth rate, $\bar{k}_i$, depends on the dimensionless breakup length z_g^b which, in turn, depends on the initial perturbation amplitude ϵR_0. Consequently, $\bar{k}_i$ depends on the initial perturbation amplitude and, either z_g^b or ϵR_0 must be provided in our model in order to compare with existing experiments. In our calculations we have fixed $z_g^b = 5$, which is a value consistent with the conditions under which the experiments of Kalaaji *et al.* (2003) were performed. Nevertheless, if the purpose of the model was to provide the breakup length given an initial perturbation amplitude ϵR_0, it could be obtained from

$$\int_0^{z_g^b} k_i(z_g)\,\mathrm{d}z_g = \frac{\ln(\epsilon)}{Re_g}. \tag{2.23}$$

Figure 4 shows the temporal amplification of disturbances for the same frequencies Ω, liquid properties and injection velocities as those used by Kalaaji *et al.* (2003) in their figure 8. In this figure, the horizontal lines represent the temporal growth rates for a liquid jet in vacuum. Note that the larger the injection velocity, the larger is the spatial amplification of disturbances, this result being a consequence of the fact that the relative importance of the aerodynamic term $(\rho_g/\rho_l)p_g$ increases with respect to the capillary one $We^{-1}f$ in (2.18) for an increasing U_l. Indeed, a simple estimation of the order of magnitude of the ratio of both terms leads to $O[(\rho_g/\rho_l)p_g/(We^{-1}f)] \sim O(We_g)$, where $We_g = (\rho_g/\rho_l)We$. Also note from this figure that the growth rates start to deviate from the solution in vacuum for gas Weber numbers as low as $We_g \sim 0.05$.

As depicted in figure 4, the computed values agree well with the experimentally measured ones, except for some dispersion shown by the latter. Thus, experimental results on the FWI breakup regime can be predicted using a linear stability analysis that retains self-consistently the effects of gas viscosity in the perturbations. It should be pointed out that the experimental growth rates corresponding to the lower injection velocities are not represented in figure 4 because, contrary to the case of high injection velocities ($\gtrsim 10\,\mathrm{m\,s^{-1}}$) of interest here, they could not be accurately measured (Kalaaji *et al.* 2003).

It is important to emphasize that the successful approach proposed by Sterling & Sleicher (1975), which is able to fit the experimental results, introduce an *ad hoc*, semi-empirical constant, whose purpose is to account for viscous effects in the gas, whereas in the present study, gas viscosity is retained self-consistently into the analysis.

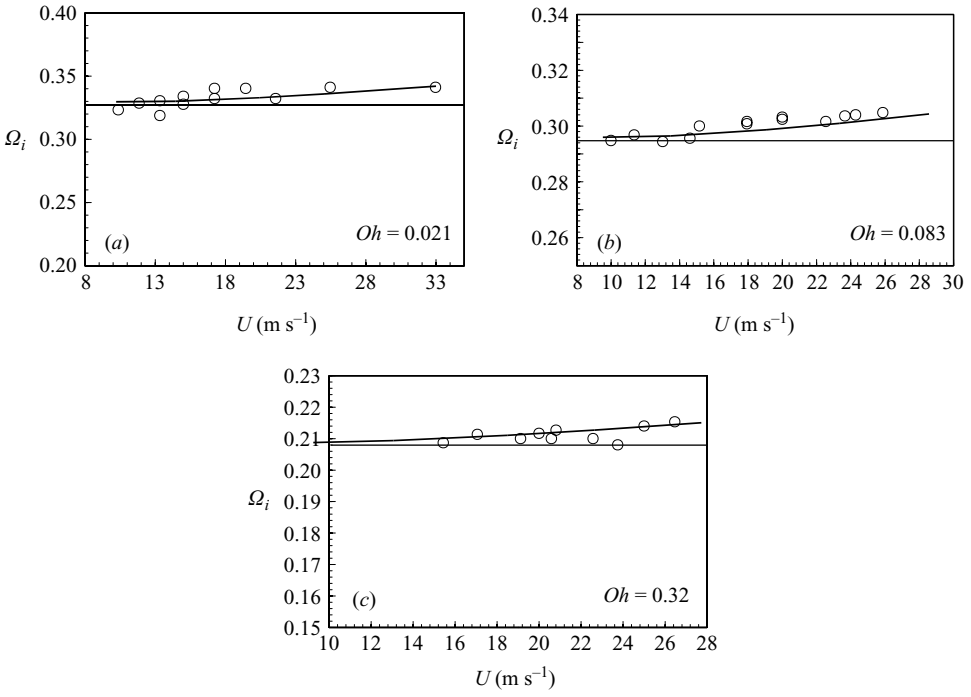

FIGURE 4. Comparison of the numerically computed (continuous line) and experimentally measured (circles) temporal growth rates. Experimental points are taken (with permission) from figure 8 of Kalaaji *et al.* (2003). The parameters corresponding to each figure are (*a*) $\rho_l = 998\,\mathrm{kg\,m^{-3}}$, $\mu_l = 10^{-3}\,\mathrm{kg\,m^{-1}\,s^{-1}}$, $\sigma = 72.9\times10^{-3}\,\mathrm{N\,m^{-1}}$, $\Omega = 0.74$; (*b*) $\rho_l = 1112\,\mathrm{kg\,m^{-3}}$, $\mu_l = 4.2\times10^{-3}\,\mathrm{kg\,m^{-1}\,s^{-1}}$, $\sigma = 70.6\times10^{-3}\,\mathrm{N\,m^{-1}}$, $\Omega = 0.68$; (*c*) $\rho_l = 1172\,\mathrm{kg\,m^{-3}}$, $\mu_l = 1.65\times10^{-2}\,\mathrm{kg\,m^{-1}\,s^{-1}}$, $\sigma = 70.1\times10^{-3}\,\mathrm{N\,m^{-1}}$, $\Omega = 0.58$. In the three cases considered, the liquid jet radius is $R = 33.3\times10^{-6}\,\mathrm{m}$ and the outer fluid properties are those corresponding to air.

However, the precise effect of gas viscosity on the development of the perturbation is not clear from the results presented so far. Indeed, gas viscosity enters into the perturbed equations in two different ways: through the basic gas velocity profiles and through the perturbed stress tensor $\boldsymbol{\tau}' = \mu_g(\nabla\boldsymbol{u}_g + \nabla^T\boldsymbol{u}_g)$. In the next section, it will be shown that both contributions must be retained in order to reproduce the experimentally measured growth rates.

3. Asymptotic analysis

It has been shown in § 2 how the experimental results on the FWI breakup regime can be both explained and reproduced by a model based on a linear spatial stability analysis of the coupled liquid–gas dynamics. Since the set of equations (2.7)–(2.18) has been fully solved numerically in the previous section under the approximation $1/Re\,\partial/\partial z_l = 0$, it is now of interest to consider such a system in some limiting cases in which there exist simpler solutions that bring to light the physics of the role of the gas viscosity in the breakup process. In this section, we carry out an asymptotic analysis of the stability equations for the gas (2.7)–(2.18) valid for large $Re_g\Omega$, being $Re_g = Re\,\nu_l/\nu_g$, and boundary-layer thickness and wavenumber, δ_g and k respectively, of the order of those found in the experimental conditions of interest here: $\delta_g/R_0 \sim O(1)$ and $k \sim O(1)$. In such a limit, the analysis shows that the effects

of viscosity in the gas perturbations are confined to a narrow layer adjacent to the gas–liquid boundary. Outside this layer, which we will call the 'Stokes layer', the perturbations are non-viscous and have been already analysed elsewhere (Gordillo *et al.* 2001). By matching the solution in the Stokes layer with that in the non-viscous region, we will deduce that the effect of the viscous perturbations in the gas stream can be accounted for by means of an approximate model which solves the spatial stability problem only for the liquid phase subject to a modified pressure boundary condition at the interface due to the presence of the gas. A similar modification was suggested in an *ad hoc* manner by Sterling & Sleicher and, therefore, our results may throw light on the physical meaning of their approximate analysis. Moreover, we will also provide a criterion to decide *a priori* whether the viscosity in the gas perturbations or, in other words, the contribution of the perturbed stress tensor $\boldsymbol{\tau}'$, should be retained in the stability analysis.

Omitting the g-subscripts, the equations governing the viscous perturbations for the gas u, v and p are

$$\mathrm{i}ku + \frac{\partial v}{\partial \xi} + \frac{v}{\xi} = 0, \tag{3.1}$$

$$-\mathrm{i}\Omega v + \mathrm{i}kUv = -\frac{\partial p}{\partial \xi} + \frac{1}{Re_g}\left(\frac{\partial^2 v}{\partial \xi^2} + \frac{1}{\xi}\frac{\partial v}{\partial \xi} - \frac{v}{\xi^2} - k^2 v - v\frac{\partial V}{\partial \xi} - V\frac{\partial v}{\partial \xi}\right), \tag{3.2}$$

$$-\mathrm{i}\Omega u + \mathrm{i}kUu + v\frac{\partial U}{\partial \xi} = -\mathrm{i}kp + \frac{1}{Re_g}\left(\frac{\partial^2 u}{\partial \xi^2} + \frac{1}{\xi}\frac{\partial u}{\partial \xi} - k^2 u - u\frac{\partial U}{\partial z_g} - V\frac{\partial u}{\partial \xi}\right), \tag{3.3}$$

where $U(\xi)$ and $V(\xi)$ are, respectively, the known unperturbed gas axial and radial velocities which depend parametrically on z_g. For large Reynolds numbers, viscous effects are confined to a narrow boundary layer adjacent to the liquid jet surface $\xi = 1$, the width of which is of order $O[(Re_g\Omega)^{-1/2}]$ as can be obtained by comparing inertia and viscous terms in the momentum equations (3.2)–(3.3). The continuity equation (3.1) then shows that, for $k \sim O(1)$, the increments in the radial component of the perturbed velocity must be $\Delta v \sim O(u/\sqrt{Re_g\Omega})$. Therefore, to analyse the viscous boundary layer it proves convenient to introduce new variables y and v^* defined as

$$y = \sqrt{Re_g\Omega}(\xi - 1), \quad v = v_l(1) + \frac{v^*}{\sqrt{Re_g\Omega}}, \tag{3.4}$$

where $v_l(1)$ is the radial liquid velocity at the free surface. In addition, for $(\xi - 1) \ll 1$, and since $1/\sqrt{Re_g\,\Omega} \ll \delta_g/R_0 \sim O(1)$, the unperturbed gas axial and radial velocities can be approximated, respectively, by

$$U(\xi) \simeq 1 + U'(1)(\xi - 1) + \cdots = 1 + \frac{1}{\sqrt{Re_g\Omega}}U'(1)y, \tag{3.5}$$

$$V(\xi) \simeq 0.5V''(1)(\xi - 1)^2 + \cdots = \frac{1}{2\,Re_g\Omega}V''(1)y^2. \tag{3.6}$$

Note that use of the continuity equation (2.2) has been made in order to deduce (3.6). On introducing the continuity equation (3.1) into (3.2)–(3.3) and expressing results in terms of the variables (3.4), we obtain the following system of equations:

$$\mathrm{i}ku = -\frac{\partial v^*}{\partial y} - v_l(1) + O\left[(Re_g\Omega)^{-1/2}\right], \tag{3.7}$$

$$\mathrm{i}[\Omega - k]\frac{\partial v^*}{\partial y} + \Omega\frac{\partial^3 v^*}{\partial y^3} = k^2 p - \mathrm{i}(\Omega - k)\,v_l(1) - \mathrm{i}kU'(1)v_l(1) + O\left[(Re_g\Omega)^{-1/2}\right], \tag{3.8}$$

$$\frac{\partial p}{\partial y} = \frac{\mathrm{i}}{\sqrt{Re_g\,\Omega}}\,(\Omega - k)\,v_l(1) + O\left(\frac{1}{Re_g\Omega}\right). \tag{3.9}$$

Observe that after (3.8)–(3.9) are solved for v^* and p, u can be obtained directly from (3.7). In order to solve for v^* and p, we use a perturbation scheme of the form

$$p = p_0 + \frac{1}{\sqrt{Re_g\Omega}}p_1, \tag{3.10}$$

where, according to (3.9), p_0 must be a constant and

$$p_1 = p_{1c} + \mathrm{i}(\Omega - k)\,v_l(1)\,y. \tag{3.11}$$

The boundary conditions for v^* in (3.8) are

$$v^*(0) = 0, \quad \frac{\partial v^*}{\partial y} = -\mathrm{i}ku(1) - v_l(1) = -\mathrm{i}k\left(u_l(1) - U'(1)\,f\right) - v_l(1), \tag{3.12}$$

where f is the perturbed jet radius and $u_l(1)$ is the liquid axial perturbed velocity at the jet surface; notice that we have made use of the continuity of longitudinal velocities across the interface (2.14). The general solution of (3.8) subjected to the boundary conditions (3.12) at $y = 0$ yield the solution

$$v^* = \frac{A}{\beta}(\mathrm{e}^{\beta y} - 1) + \frac{B}{\mathrm{i}(\Omega - k)}y, \tag{3.13}$$

where we have defined the constants

$$\beta \equiv \exp\left(\mathrm{i}\left(\frac{3\pi}{4} + \frac{\gamma}{2}\right)\right)\sqrt{\frac{|\,\Omega - k\,|}{\Omega}}, \tag{3.14}$$

with $\gamma = \arg((\Omega - k)/\Omega)$ such that $Re(\beta) < 0$, and

$$B = k^2 p_0 - \mathrm{i}(\Omega - k)v_l(1) - \mathrm{i}kU'(1)v_l(1), \tag{3.15}$$

$$A = -\mathrm{i}k[u_l(1) - U'(1)\,f] - v_l(1) - \frac{B}{\mathrm{i}(\Omega - k)}. \tag{3.16}$$

Note that the constants p_0 and p_{1c} will be obtained from the matching with the outer solution. In the limit $y \to \infty$,

$$v(y \to \infty) \to v_l(1) + \frac{B}{\mathrm{i}(\Omega - k)}(\xi - 1) - \frac{1}{\sqrt{Re_g\Omega}}\frac{A}{\beta}, \tag{3.17}$$

$$p(y \to \infty) \to p_0 + \mathrm{i}(\Omega - k)v_l(1)(\xi - 1) + \frac{p_{1c}}{\sqrt{Re_g\Omega}}. \tag{3.18}$$

Equation (3.17) reveals that, outside the Stokes layer, the radial velocity suffers an increment $-A/(\sqrt{Re_g\,\Omega}\,\beta)$ with respect to that at the free surface, $v_l(1)$. As will be shown below, this term introduces a correction for the gas pressure at the free surface of the order of $1/\sqrt{Re_g(\Omega - k)}$.

Outside the boundary layer analysed above, viscous effects are negligible in the perturbations and equations (3.2)–(3.3) can be written as

$$\frac{1}{\xi}\frac{\partial}{\partial \xi}\left(\xi\frac{\partial p}{\partial \xi}\right) - k^2 p = -2\mathrm{i}kU'v, \tag{3.19}$$

$$v = \frac{\mathrm{i}}{kU - \Omega}\frac{\partial p}{\partial \xi}, \tag{3.20}$$

where we have neglected terms of order $O[(Re_g\Omega)^{-1}L(v)]$, $L(v)$ representing linear expressions of v and its derivatives. From (3.19)–(3.20) we also obtain the following differential equation for p

$$\frac{\partial^2 p}{\partial \xi^2} = k^2 p - \left(\frac{2kU'}{\Omega - kU} + \frac{1}{\xi}\right)\frac{\partial p}{\partial \xi}, \tag{3.21}$$

where terms of order $O[(Re_g\Omega)^{-1}]$ have also been neglected; as shown in Gordillo *et al.* (2001), the solution of (3.21) which is bounded at $\xi \to \infty$ must satisfy at $\xi = 1$ the condition

$$P(\Omega, k) \equiv \frac{p(1)}{p'(1)} = -\int_1^\infty \frac{1}{\xi}\frac{1}{n^2(\xi)}\left[\frac{Uk - \Omega}{U(1)k - \Omega}\right]^2 \mathrm{d}\xi, \tag{3.22}$$

where $n(\xi)$ is the particular solution of (3.21) which satisfies the boundary conditions $n(1) = 1$ and $n'(1) = 0$. Equations (3.19)–(3.20) can be solved using the following perturbation scheme

$$v = w_1(\xi) + \frac{1}{\sqrt{Re_g\Omega}} w_2(\xi), \tag{3.23}$$

$$p = \Pi_1(\xi) + \frac{1}{\sqrt{Re_g\Omega}} \Pi_2(\xi), \tag{3.24}$$

where v and p in (3.23)–(3.24) must match the behaviours (3.17)–(3.18) at $\xi \to 1$. To accomplish this we expand (3.23)–(3.24) around $\xi = 1$ in the form

$$v = [w_1(1) + w_1'(1)(\xi - 1)] + \frac{1}{\sqrt{Re_g\Omega}} w_2(1), \tag{3.25}$$

$$p = [\Pi_1(1) + \Pi_1'(1)(\xi - 1)] + \frac{1}{\sqrt{Re_g\Omega}} \Pi_2(1). \tag{3.26}$$

Observe that, since both $\Pi_1(\xi)$ and $\Pi_2(\xi)$ satisfy (3.21), condition (3.22) implies that

$$\frac{\Pi_1(1)}{\Pi_1'(1)} = \frac{\Pi_2(1)}{\Pi_2'(1)} = P. \tag{3.27}$$

After some algebraic computations using (3.19)–(3.21), comparison of (3.25) with (3.17) and (3.26) with (3.18) yields

$$p_0 = \Pi_1'(1)P = \mathrm{i}(\Omega - k)P v_l(1), \tag{3.28}$$

$$p_{1c} = \Pi_2'(1)P = \mathrm{i}P(\Omega - k)(-A/\beta). \tag{3.29}$$

Therefore, the perturbed pressure at $\xi = 1$, which quantifies the aerodynamic effect of the surrounding gaseous atmosphere, can be approximated by

$$p(1) = p_0 + (Re_g\Omega)^{-1/2} p_{1c} = \mathrm{i}(\Omega - k)v_l(1)P[1 + \alpha] + O[[Re_g(\Omega - k)]^{-1}], \tag{3.30}$$

where α is given by

$$\alpha = \frac{1}{\sqrt{-\mathrm{i}Re_g(\Omega - k)}}\left(Pk^2 + \frac{\mathrm{i}ku_l(1)}{v_l(1)}\right), \tag{3.31}$$

with $Re[\sqrt{-\mathrm{i}Re_g(\Omega - k)}] < 0$ in (3.31). Note that use of the kinematic free-surface condition $v_l(1) = -\mathrm{i}\, f\,(\Omega - k)$ has been made in order to deduce (3.30). Thus, once P

is computed using (3.22), the gas pressure over the liquid jet can be calculated through the asymptotic equation (3.30) as a function of $u_l(1)$, $v_l(1)$, Ω, k and Re_g. Notice that the two different contributions of gas viscosity on the aerodynamic effect are clearly differentiated in (3.30). Indeed, the only term that explicitly incorporates the influence of the gas velocity profile in (3.30) is P, which results of solving the inviscid equation (3.21). Furthermore, the effect of retaining viscous diffusion into the perturbed equations (3.1)–(3.3) can be evaluated, with errors $\sim O([Re_g(\Omega-k)]^{-1})$ through (3.31). Consequently, since P strongly depends on $U_g(\xi)$ (see (3.22)), a correct estimation of the aerodynamic effect requires us to perform the stability analysis using realistic basic velocity profiles. Moreover, the condition which, in view of (3.30) permits us to safely neglect viscosity in the perturbed equations, is $|\alpha| \ll 1$, α being defined in (3.31). Also note that, if $Re_g(\Omega-k) \sim O(1)$, viscous diffusion must be retained in the stability equations since, from (2.10), we have $O[(\Omega-k)u_g] \sim O(v_g \partial U_g/\partial\xi) \sim O(1/Re_g \partial^2 u_g/\partial\xi^2)$ and, consequently, we would commit order-unity errors if we neglected the perturbed viscosity terms from the stability equations. Observe that the criterion $|\alpha| \ll 1$, with α computed *a priori* using only the much simpler inviscid stability results should still serve as a guide to assess the accuracy of a stability analysis in which viscous diffusion is neglected (see, for instance, Villermaux 1998; Gordillo *et al.* 2001; Marmottant & Villermaux 2004; Boeck & Zaleski 2005). Note that the value of α can be calculated readily from the inviscid stability results, as follows. Once the values of k, $u_l(1)$ and $v_l(1)$ are computed from the inviscid spatial stability analysis, P is calculated from the integral (3.22). Finally, α is given by simply substituting the results obtained into (3.31). However, (3.30) also indicates that, owing to $O[u_l(1)/v_l(1)] \sim O(1)$, the criterion to ensure the validity of an inviscid stability analysis in the cases in which $O(P) \sim O(1)$, is simply $|Re_g(\Omega-k)| \gg 1$ and thus, the exact calculation of P can be avoided.

In order to validate the asymptotic equation (3.30), the exact value of the gas pressure at the gas–liquid interface, p_E, will be compared with those obtained through different approximations. On the one hand, p_E will be calculated through the numerical procedure described in § 2 and, on the other hand, we will compute the approximations $p_I = \mathrm{i}(\Omega-k)v_l(1)P$ and $p_V = p_I(1+\alpha)$ obtained, respectively, by neglecting and retaining α in (3.30). Furthermore, the gas pressure provided by the Sterling & Sleicher (1975) model, represented as p_{SS} and given by

$$p_{SS}(1) = 0.175\,\mathrm{i}(\Omega-k)v_l(1)\frac{\Omega^2}{(\Omega-k)^2}P = 0.175\,\mathrm{i}(\Omega-k)v_l(1)\frac{\Omega^2}{(\Omega-k)^2}\frac{-K_0(k)}{kK_1(k)}, \quad (3.32)$$

will also be compared with p_E. In (3.32), $P \equiv p(1)/p'(1) = -K_0(k)/k\,K_1(k)$ since the Sterling & Sleicher (1975) model assumes an uniform gas velocity profile. Also notice that p_I, p_V and p_{SS} will be computed taking k, $u_l(1)$ and $v_l(1)$ from the numerical solution already obtained in the previous section.

Table 1 shows the comparison of p_E with p_I (gas pressure at the interface if viscous diffusion is neglected in the perturbed equations) for increasing values of the liquid Reynolds number. From this table, note that the relative error, $\epsilon_I = (p - p_I)/p$ is $\sim O(\alpha)$, in accordance with (3.30). Consequently, since the relative error ϵ_I remains significant even for Reynolds numbers as large as 10^5, viscous diffusion must be retained into the stability equations in order to describe properly the FWI breakup regime. Note that the relative error ϵ_I does not scale with $1/\sqrt{Re_g}$, but with $1/\sqrt{Re_g(\Omega-k)}$ as shown in (3.30). Indeed, $O(1/\sqrt{Re_g}) \ll O[1/\sqrt{Re_g(\Omega-k)}]$

Re	p_E	p_I	$\lvert\epsilon_I\rvert$	$\lvert\alpha\rvert$
10^5	$-5.41\times10^{-3}-\mathrm{i}\,1.15\times10^{-2}$	$-2.54\times10^{-3}-\mathrm{i}\,1.12\times10^{-2}$	2.3×10^{-1}	3.33×10^{-1}
10^6	$-4.01\times10^{-3}-\mathrm{i}\,1.22\times10^{-2}$	$-2.79\times10^{-3}-\mathrm{i}\,1.23\times10^{-2}$	9.5×10^{-2}	1.05×10^{-1}
10^7	$-3.41\times10^{-3}-\mathrm{i}\,1.30\times10^{-2}$	$-3\times10^{-3}-\mathrm{i}\,1.31\times10^{-2}$	3.14×10^{-2}	3.32×10^{-2}

TABLE 1. Comparison of the gas pressure at the interface for an air–water jet for increasing Reynolds numbers using different approximations. $We=50$, $Oh=0.021$, $z_g=2.2$, $\Omega=0.74$.

Re	p_E	p_V	$\lvert\epsilon_V\rvert$	$\lvert\alpha\rvert$
10^5	$-5.41\times10^{-3}-\mathrm{i}\,1.15\times10^{-2}$	$-6.18\times10^{-3}-\mathrm{i}\,1.01\times10^{-2}$	1.35×10^{-1}	3.33×10^{-1}
10^6	$-4.01\times10^{-3}-\mathrm{i}\,1.22\times10^{-2}$	$-4.06\times10^{-3}-\mathrm{i}\,1.19\times10^{-2}$	2.34×10^{-2}	1.05×10^{-1}
10^7	$-3.41\times10^{-3}-\mathrm{i}\,1.30\times10^{-2}$	$-3.43\times10^{-3}-\mathrm{i}\,1.30\times10^{-2}$	2.9×10^{-3}	3.32×10^{-2}

TABLE 2. Comparison of the gas pressure at the interface for an air–water jet for increasing Reynolds numbers using different approximations. $We=50$, $Oh=0.021$, $z_g=2.2$, $\Omega=0.74$.

Re	p_E	p_{SS}
10^5	$-5.41\times10^{-3}-\mathrm{i}\,1.15\times10^{-2}$	$-3.33\times10^{-2}-\mathrm{i}\,1.52\times10^{-3}$
10^6	$-4.01\times10^{-3}-\mathrm{i}\,1.22\times10^{-2}$	$-3.65\times10^{-2}-\mathrm{i}\,1.67\times10^{-3}$
10^7	$-3.41\times10^{-3}-\mathrm{i}\,1.30\times10^{-2}$	$-3.92\times10^{-2}-\mathrm{i}\,1.80\times10^{-3}$

TABLE 3. Value of the gas pressure using (3.32) for the same conditions as those indicated in tables 1 and 2.

since, for the high-Weber-number flows considered here, $\partial k_r/\partial\Omega\simeq1\rightarrow\Omega_r\simeq k_r$, and $O(k_i)\sim O(We^{-1/2})\ll1$; consequently, $|\Omega-k|\ll1$ and $Re_g\gg Re_g|\Omega-k|$.

A further check on the validity of the asymptotic analysis is provided in table 2, where p_V is compared with p_E. In this case, the relative error $\epsilon_V=(p-p_V)/p$ is much smaller than α for sufficiently large values of the Reynolds number, consistent with the asymptotic analysis.

Finally, p_{SS} is compared with p_E in table 3 in order to check the accuracy of the Sterling & Sleicher model. As can be deduced by comparing (3.30) and (3.32), their approach of modelling gas viscosity through an *ad hoc* multiplicative factor seems to be qualitatively correct but, from this table, note that the values of p_{SS} differ by an order of magnitude from the exact ones. This disagreement arises because both basic gas velocity profile and gas Reynolds number vary from one experimental situation to another, whereas the Sterling & Sleicher (1975) multiplicative factor does not. This result is in contradiction to the success of Sterling & Sleicher's model in predicting experimental results (see Kalaaji *et al.* 2003; González & García 2004). A plausible explanation for this disagreement is provided in figure 5, where the correct value of the multiplicative factor, F, which is defined as

$$F=p_E\left[\mathrm{i}(\Omega-k)v_l(1)\frac{\Omega^2}{(\Omega-k)^2}\,\frac{-K_0(k)}{k\,K_1(k)}\right]^{-1},\tag{3.33}$$

is represented as a function of the intact jet length, z_g. Notice that, under the realistic experimental conditions for which the multiplicative factor is represented in figure 5, F is no longer real and, in addition, evolves downstream. However, the mean value

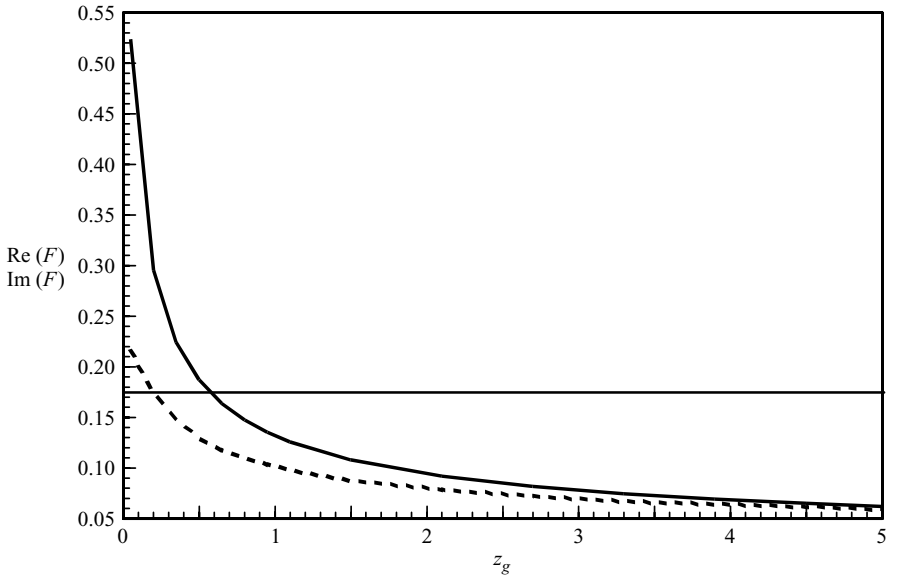

FIGURE 5. Factor F, calculated (3.33) with the numerical values computed from the following set of values for the parameters: $We = 450$, $Oh = 0.021$, $\Omega = 0.74$. Continuous and dotted lines indicate, respectively, real and imaginary parts of F. Physical properties of water (see caption to figure 3) and air. The horizontal line is placed at 0.175.

of its modulus,

$$|\bar{F}| = \frac{1}{z_g^b} \int_0^{z_g^b} |F| \, \mathrm{d}z_g = 0.14, \tag{3.34}$$

which is fairly close to the value $F = 0.175$ used by Sterling & Sleicher (1975). Consequently, the Sterling & Sleicher (1975) factor may be interpreted as a measure of the mean variation of the basic velocity profiles and viscous diffusion in the perturbations along the intact length of the jet.

Finally, note that the asymptotic analysis performed in this section give good results only for very large Reynolds numbers. Since experiments are usually performed at much lower Reynolds numbers, in general, we must resort to the complete numerical analysis described in the previous section for the prediction of experimental growth rates. Nevertheless, the relevance of the asymptotics stems from the fact that it clarifies the role of gas viscosity in the development of the instability and, in addition, it permits us to identify a parameter, α, which provides us with a criterion to determine the validity of inviscid linear stability analysis.

4. Conclusions

In this paper we have studied the breakup of a liquid jet discharging in a stagnant atmosphere. In order to treat the effect of gas viscosity rigorously, we have performed a linear spatial stability analysis in which viscosity is retained self-consistently in the gas perturbations. For this purpose, we have computed the downstream evolution of the gas velocity profiles induced by the liquid jet and have retained in the stability equations viscous diffusion terms $\sim O(1/Re)$. The numerically obtained perturbation growth rates are computed under the approximation $1/Re\,\partial/\partial z_l = 0$ by discretizing the coupled gas–liquid stability equations using a Chebychev spectral collocation

method (Lin & Chen 1998; Yecko *et al.* 2002) and solving them through the matrix companion method (Bridges & Morris 1984). The stability of both axisymmetric ($m = 0$) and helicoidal ($m = 1$) modes has been considered and the results show that asymmetric disturbances may grow faster than axisymmetric ones only for sufficiently large values of both the Weber and Ohnesorge numbers. The numerical growth rates for axisymmetric disturbances are compared with experiments, and an excellent agreement is obtained. This permits us to conclude that a simple stability analysis such as the one presented here can be used to predict experimental results.

In addition, in order to elucidate the precise role of gas viscosity into the problem, we have performed an asymptotic analysis valid for axisymmetric disturbances, which shows that, for sufficiently large values of the Reynolds number, viscous effects in the perturbations are confined within a 'Stokes layer' adjacent to the liquid–gas interface. Moreover, the resulting asymptotic expression for the gas pressure at the liquid interface, which reflects the influence of the aerodynamic effect of the surrounding gaseous atmosphere on the liquid jet, permits us to differentiate clearly the influence of both the basic velocity profile and viscous diffusion in the development of the instability. It is found that, for sufficiently high Reynolds numbers, the asymptotic results are in agreement with the exact numerical ones up to terms of order $|\alpha| \ll 1$, where α is the parameter defined in (3.31) which measures the relative importance of viscosity in the gas perturbations. The parameter α can be computed *a priori* using solely inviscid stability results and its smallness constitutes a criterion to assess the validity of the simpler non-viscous stability analysis. A similar criterion can easily be deduced in other physical situations such as those arising in the study of the atomization of liquid jets with high-speed coflowing gas streams. Equation (3.30) also indicates that, in the cases in which $O(P) \sim O(1)$, the criterion to ensure the validity of an inviscid stability analysis is simply $|Re_g(\Omega - k)| \gg 1$.

Finally, asymptotics also reveals that, for sufficiently high Re, the complete analysis can be simplified to solve the stability equations in the liquid region subject to a modified pressure boundary condition which takes into account the presence of the gas. This resembles the treatment given to the problem by Sterling & Sleicher (1975), although in our paper both the result and the limits of validity have been obtained in a self-consistent manner. Although the results of the asymptotic analysis are valid only for Reynolds numbers which are too large to be compared with experiments, its relevance stems from the fact that it clarifies the role played by gas viscosity in the development of instabilities and, in addition, it permits us to identify a parameter, α, which provides us with a criterion to determine the validity of inviscid linear stability analysis. In general, in order to predict results under realistic experimental conditions we must solve numerically the complete set of linear stability equations of § 2 corresponding to the coupled liquid–gas problem which self-consistently retains viscosity effects in the gas perturbations.

The authors greatly acknowledge P. Attanè for providing us with helpful experimental information. They would also like to thank H. González and J. García for their careful reading of the manuscript and helpful suggestions.

REFERENCES

Ambravaneswaran, B., Phillips, S. & Basaran, O. A. 2000 Theoretical analysis of a dripping faucet. *Phys. Rev. Lett.* **85**, 5332–5335.

Ambravaneswaran, B., Subramani, H. J., Phillips, S. D. & Basaran, O. A. 2004 Dripping–jetting transitions in a dripping faucet. *Phys. Rev. Lett.* **93**, 034501(1–4).

Bertolotti, F., Herbert, T. & Spalart, P. 1992 Linear and nonlinear stability of the Blasius boundary layer. *J. Fluid Mech.* **242**, 441–474.

Boeck, T. & Zaleski, S. 2005 Viscous vs. inviscid instability of two-phase mixing layers with continuous velocity profile. *Phys. Fluids* **17**, 032106(1–11).

Bridges, J. & Morris, P. J. 1984 Differential eigenvalue problems in which the parameter appears nonlinearly. *J. Comput. Phys.* **437**, 222–224.

Clanet, C. & Lasheras, J. 1999 Transition from dripping to jetting. *J. Fluid Mech.* **383**, 307–326.

Fernández-Feria, R. 1999 Nonparallel linear stability analysis of longs vortex. *Phys. Fluids* **11**, 1114–1126.

Gaster, M. 1962 A note on the relation between temporally-increasing and spatially-increasing disturbances in hydrodynamic stability. *J. Fluid Mech.* **14**, 222–224.

González, H. & García, F. J. 2004 Comment on breakup length of forced liquid jets [*Phys. Fluids* **15**, 2469 (2003)]. *Phys. Fluids* (submitted).

Gordillo, J. & Pérez-Saborid, M. 2002 Transient effects in the signalling problem. *Phys. Fluids* **14**, 4329–4343.

Gordillo, J., Pérez-Saborid, M. & Gañán Calvo, A. 2001 Linear stability of co-flowing liquid–gas jets. *J. Fluid Mech.* **448**, 23–51.

Hoyt, J. & Taylor, J. 1977 Waves on water jets. *J. Fluid Mech.* **83**, 119–127.

Huerre, P. & Monkewitz, P. 1990 Local and global instabilities in spatially developing flows. *Annu. Rev. Fluid Mech.* **22**, 473–537.

Kalaaji, A., Lopez, B., Attane, P. & Soucemarianadin, A. 2003 Breakup length of forced liquid jets. *Phys. Fluids* **15**, 2469–2479.

Keller, J. B., Rubinow, S. I. & Tu, Y. O. 1973 Spatial instability of a jet. *Phys. Fluids* **16**, 2052–2055.

Lasheras, J. & Hopfinger, E. 2000 Liquid jet instability and atomization in a coaxial gas stream. *Annu. Rev. Fluid Mech.* **32**, 275–308.

Le Dizès, S. 1997 Global modes in falling capillary jets. *Eur. J. Mech.* B/*Fluids* **16**, 761–778.

Lin, S. & Chen, J. 1998 Role played by the interfacial shear in the instability mechanism of a viscous liquid jet surrounded by a viscous gas in a pipe. *J. Fluid Mech.* **376**, 37–50.

Lin, S. & Lian, Z. 1989 Absolute instability of a liquid jet in a gas. *Phys. Fluids* A **1**, 490–493.

Lin, S. & Reitz, R. 1998 Drop and spray formation from a liquid jet. *Annu. Rev. Fluid Mech.* **30**, 85–105.

Lozano, A., Barreras, F., Hauke, G. & Dopazo, C. 2001 Longitudinal instabilities in an air-blasted liquid sheet. *J. Fluid Mech.* **437**, 143–173.

Marmottant, P. & Villermaux, E. 2004 On spray formation. *J. Fluid Mech.* **498**, 73–111.

Olendraru, C., Sellier, A., Rossi, M. & Huerre, P. 1999 Inviscid instability of the Batchelor vortex: absolute-convective transition and spatial branches. *Phys. Fluids* **11**, 1805–1820.

Rayleigh, Lord 1878 On the instability of jets. *Proc. Lond. Math. Soc.* **10**, 4–13.

Reitz, R. & Bracco, F. 1982 Mechanism of atomization of a liquid jet. *Phys. Fluids* **25**, 1730–1742.

Rodríguez-Rodríguez, J., Sánchez, A. & Martínez-Bazán, C. 2004 The boundary-layer flow induced by a flat plate emerging normally to a wall. *Heat Mass Transfer* **40**, 959–962.

Sterling, A. & Sleicher, C. 1975 The instability of capillary jets. *J. Fluid Mech.* **68**, 477–495.

Tutty, O., Price, W. & Parsons, A. 2002 Boundary layer flow on a long thin cylinder. *Phys. Fluids* **14**, 628–637.

Villermaux, E. 1998 Mixing and spray formation in coaxial jets. *J. Prop. Power* **14**, 807–817.

Weber, C. 1931 On the breakdown of a fluid jet. *Z. Angew. Math. Mech.* **11**, 136–141.

Yang, H. 1992 Asymmetric instability of a liquid jet. *Phys. Fluids* A **4**, 681–689.

Yecko, P., Zaleski, S. & Fullana, J. 2002 Viscous modes in two-phase mixing layers. *Phys. Fluids* **14**, 4115–4122.

Yoon, S. & Heister, S. 2004 A nonlinear atomization model based on a boundary layer instability mechanism. *Phys. Fluids* **16**, 47–61.